Available online at www.sciencedirect.com
ScienceDirect
Journal of Nuclear Materials 374 (2008) 270–280
journal of nuclear materials
www.elsevier.com/locate/jnucmat

Microstructure tailoring for property improvements by grain boundary engineering

L. Tan [a,*], K. Sridharan [a], T.R. Allen [a], R.K. Nanstad [b], D.A. McClintock [b]

[a] University of Wisconsin-Madison, Madison, WI 53706, USA
[b] Oak Ridge National Laboratory, Oak Ridge, TN 37831, USA

Received 25 June 2007; accepted 15 August 2007

Abstract

Grain boundary engineering (GBE) was employed to improve materials properties such as corrosion resistance and strength by optimizing the grain boundary character distribution. Two high-temperature alloys, designated Incoloy 800H and Inconel 617 were selected in this study due to their potential applications for the Generation IV nuclear power systems. The GBE treatments on the alloys 800H and 617 were accomplished by a series of thermomechanical processing. The effect of the GBE treatments on the corrosion resistance and mechanical properties of the materials were evaluated using supercritical water exposure tests, cyclic oxidation tests, impact tests, and tensile tests. The microstructures of the tested samples were analyzed by means of optical microscopy, scanning electron microscopy, energy-dispersive X-ray spectroscopy, electron backscatter diffraction, X-ray photoelectron spectroscopy, and grazing incidence X-ray diffraction. The results indicate that the GBE treatments greatly mitigated the oxide exfoliation of the alloy 800H and reduced the oxidation rate of the alloy 617. The GBE treatment also greatly enhanced the strength of alloy 800H at room temperature (e.g. impact tests) and high-temperatures (e.g. tensile tests after neutron irradiation), but did not significantly impair the material's ductility.

PACS: 81.65.Mq; 81.40.Lm; 66.30.−h; 61.72.Mm; 82.33.De

1. Introduction

Grain boundaries are common defects existing in crystalline materials, and play a major factor in determining the physical, mechanical, electrical, and chemical properties of crystalline materials [1]. Based on the misorientation between adjacent grains, grain boundaries can be categorized as low-angle boundaries (LABs) with a misorientation angle generally less than 15° and high-angle boundaries (HABs). Using the concept of the coincidence site lattice (CSL), they also can be categorized as $\Sigma 1$ (maximum misorientation angle 15°) boundaries corresponding to the LABs [2], and low-Σ CSL boundaries (CSLBs, $3 \leqslant \Sigma \leqslant 29$) and random boundaries corresponding to the HABs. The Σ is a value defined as the reciprocal density of coincident sites at the grain boundary between two adjoining grains.

Compared to random boundaries, low-Σ CSLBs have many special properties such as low boundary energy, less susceptibility to impurity or solute segregation, and greater resistance to grain boundary sliding and intergranular degradation [2]. Due to the special properties of the low-Σ CSLBs, grain boundary engineering (GBE) was proposed as an approach to control the properties of polycrystalline metals by tuning grain boundary character distribution (GBCD) to obtain a high fraction of low-Σ CSLBs and interrupt the connectivity of random boundaries. GBE has been used to improve the properties of polycrystalline metals such as strength [3], creep [4], weldability [5], and stress corrosion cracking [6]. Among the low-Σ CSLBs, the contribution of $\Sigma 3$ boundaries to the property improvements has

* Corresponding author. Tel.: +1 608 262 7476; fax: +1 608 263 7451.
E-mail address: lizhentan@wisc.edu (L. Tan).

0022-3115/$ - see front matter © 2007 Elsevier B.V. All rights reserved.
doi:10.1016/j.jnucmat.2007.08.015

been found to be the most significant [7,8]. This is because the energy of $\Sigma 3$ boundaries is extremely low, typically about 1/50 of a random boundary [2]. Detailed information about the CSL model and CSL effect on GBE can be found in Ref. [2].

Successful GBE by means of thermomechanical processing has been applied to face-centered-cubic (FCC) materials with low stacking-fault-energies. Thermomechanical processing is a combination of deformation and annealing to produce annealing twins. The applied thermomechanical processing can generally be categorized as recrystallization, featuring a high level of cold work followed by a short high temperature anneal, and strain annealing, featuring a low level of cold work followed by a long medium/high temperature anneal [9].

Incoloy alloy 800H (UNS N08810, Fe–31Ni–20Cr) and Inconel alloy 617 (UNS N06617, Ni–22Cr–13Co–9Mo) were studied in this work due to their potential applications in the Generation IV Nuclear Power Systems [10]. The detailed specifications of these two alloys regarding the physical and mechanical properties could be found in Ref. [11]. Both of these alloys are solid-solution-strengthened alloys with additional strengthening by precipitation of titanium nitrides and carbides such as MC (rich in Ti), $M_{23}C_6$ (rich in Cr), and M_6C (rich in Ni and Mo in alloy 617). Titanium nitrides are stable at all temperatures below the melting point and are therefore unaffected by heat treatment [11]. Furthermore, the γ'-phase such as $Ni_3(Al, Ti)$ was observed in alloy 617 at temperatures between 650 and 760 °C [11]. Both of these two alloys have good creep resistance. However, extensive oxide exfoliation was observed on alloy 800H following exposure to supercritical water (SCW) [12]. The corrosion resistance of alloy 617 was found inappropriate for very high temperature reactor (VHTR) application [13]. This study was performed primarily to improve the corrosion resistance of these alloys by means of GBE with limited testing to investigate the effect of GBE on radiation response.

SCW is an attractive superfluid existing at temperatures and pressures above the critical point of water at 374 °C and 22.1 MPa. It has been used in modern power plants to improve thermal efficiency and reduce the release of deleterious gases such as carbon dioxide, nitrogen oxides, and sulfur oxides. Due to these advantages, SCW has been proposed as a coolant for Generation IV nuclear power plants [10]. Preliminary SCW exposure tests indicated that GBE could be an effective approach to mitigate oxide exfoliation of alloy 800H at 500 °C [12]. This paper presents the effect of GBE on the corrosion resistance and strength of alloys 800H and 617.

2. Experiments

The materials used in this study were commercial alloys Incoloy 800H and Inconel 617 and the chemical compositions provided with the materials are listed in Table 1. Both of the as-received alloys were annealed at ~1177 °C for a time commensurate with section size followed by water quenching. Thermomechanical processing was performed on the as-received samples cut from the alloys by a series of a low level of cold work followed by a high temperature anneal and water quenching. Based on the previous experience [14,15], a series of thermomechanical processing with a ~6% thickness reduction followed by annealing at 1050 °C for 90 min for alloy 800H and a ~5% thickness reduction followed by annealing at 1100 °C for 90 min for alloy 617 were employed for the GBE treatments.

2.1. Supercritical water (SCW) exposure tests

The as-received and the GBE-treated alloys 800H and 617 were subjected to SCW exposure tests. Rectangular samples (31.7 mm × 12.7 mm) with a thickness of ~1 mm were cut from the as-received and the GBE-treated materials then polished down to a 1 μm surface finish and ultrasonically cleaned prior to the exposure. The SCW was maintained at 500 or 600 °C and ~25 MPa with a test section inlet dissolved oxygen content of ~25 ppb and a flow rate of ~1 m/s. The applied heating and cooling rates were ~1 °C/min.

2.2. Cyclic oxidation tests

Cyclic oxidation testing is a key method to aid material selection and to predict service lifetime of components. The as-received and the GBE-treated alloys 800H and 617 samples were subjected to cyclic oxidation testing in air at a variety of temperatures such as 500 and 850 °C for the 800H samples and 850 and 1000 °C for the 617 samples. Two as-received and two GBE-treated samples were tested at the same time for each alloy at a designated cyclic exposure temperature. Each cycle was composed of putting samples in a furnace at designated temperatures for a heating period of one day and followed by pulling samples out for an air cooling to room temperature for about 15 min to measure the weight changes. An electronic balance with a sensitivity of 0.1 mg was employed.

Table 1
Chemical composition (wt%) of Incoloy 800H and Inconel 617

Alloy	Fe	Cr	Ni	Co	Mo	Mn	Cu	Si	Ti	Al	Others
800H	45.26	20.42	31.59	–	–	.76	.42	.13	.57	.50	C, S, P
617	1.47	22.05	52.32	12.69	9.35	.27	.11	.15	.38	1.07	C, S, B

2.3. Impact tests

An INSTRON Dynatup drop weight impact test machine (model 8200) was employed for the impact tests of the alloy 800H specimens in the as-received and the GBE-treated conditions. The test specimens, 2.5 mm × 10 mm × 55 mm (width × height × length) with a standard V-notch, were fabricated by following the sub-size specimen configuration described in ASTM E 23-06 [16]. A load of 15 kg and an impact velocity of 2.3 m/s were employed for the impact tests at room temperature.

2.4. Tensile tests

Small tensile test specimens with a gauge section of 1.5 mm × 0.76 mm × 7.6 mm (width × thickness × length) were cut from alloy 800H in the as-received and the GBE-treated conditions. Two sets of the as-received and the GBE-treated specimens were irradiated in the High Flux Isotope Reactor (HFIR) at Oak Ridge National Laboratory in specially designed 'rabbit' capsules. The capsules were designed to obtain irradiation temperatures of 600 and 750 °C with a total dose of 1.2 and 1.6 displacements per atom (dpa), respectively. SiC temperature monitors were included inside each capsule so the actual temperatures the specimens experienced during irradiation could be accurately measured. Following irradiation the actual irradiation temperatures were determined for each capsule utilizing electrical resistivity measurements of the SiC monitors between annealing treatments; this method has been used extensively for rabbit capsule irradiations and has been shown to provide an accuracy of about ±20 °C [17]. The measured actual irradiation temperatures for the capsules were found to be 580 and 660 ± 20 °C. The neutron-irradiated tensile specimens were tested at their respective irradiation temperatures at a strain rate of 10^{-3} 1/s.

2.5. Microstructure characterization

A LEO 1530 field-emission scanning electron microscope (FESEM) was the major analytical tool employed in this study for microstructural characterization. This FESEM is equipped with energy-dispersive X-ray spectroscopy (EDS) and electron backscatter diffraction (EBSD) capability. EBSD was employed for determining grain boundary misorientation using the TexSEM Laboratories (TSL) orientation imaging microscopy (OIM) system MSC2200. To obtain good quality EBSD data, the samples were polished with SiC abrasive paper down to 1200 grit followed by sequential polishing with 1 μm diamond paste, alpha alumina, and colloidal silica solutions. The SEM was operated at 20 kV, and the automatic EBSD area scan was performed using a hexagonal grid with a variety of step sizes depending upon the microstructure of the examined materials.

In addition to the SEM/EDS/EBSD, other techniques such as optical microscopy for surface morphology, X-ray photoelectron spectroscopy (XPS) for oxide surface chemistry, and grazing-incidence X-ray diffraction (GIXRD) for oxide phase identification were employed in this study.

3. Results and discussion

3.1. Grain boundary engineering (GBE)

The GBE-treatments performed on the alloys 800H and 617 did not change the grain size and hardness of the materials as statistically measured by EBSD mapping and the Vicker's micro-hardness. Coherent twins were not counted as grain boundaries during the grain size calculation because they are immobile and not a constituent of the intergranular transport network [14]. At the GBE treatment temperatures such as 1050 °C for the alloy 800H and 1100 °C for the alloy 617, only carbides may be changed by the GBE treatments since carbides such as $Cr_{23}C_6$ start to form at temperatures below ~1100 °C according to thermodynamic calculations. However, distinct thermal segregation and precipitation probability were not introduced by the GBE treatments as evaluated by scanning Auger microscopy analyses on in situ fractured samples. The only significant change induced by the GBE-treatments is the grain boundary character distribution (GBCD).

3.1.1. Grain boundary character distribution (GBCD)

The GBCD of the as-received and the GBE-treated alloys 800H and 617 samples are plotted in a triangle (an adapted ternary phase diagram) as shown in Fig. 1(a) with the three axes denoting the fraction of the $\Sigma 1$, low-Σ CSL, and random boundaries. The GBE treatment greatly increased the fraction of low-Σ CSLBs and decreased the fraction of random boundaries. The fraction of low-Σ CSLBs with Σ from 3 to 29 of the as-received and the GBE-treated alloy 800H and alloy 617 samples is shown in Fig. 1(b). The fraction of annealing twin boundaries $\Sigma 3$ and its twin variants $\Sigma 9$ and $\Sigma 27$ had been greatly increased by the GBE treatment. The fraction of $\Sigma 3$ boundaries of the GBE-treated alloy 617 samples was enhanced to ~64% which is approaching the theoretical twin limit of 2/3 [18].

3.1.2. Thermal stability of the GBE-treated samples

Since atomic migration is increased at elevated temperatures, the GBE-promoted low-Σ CSLBs may become unstable and be transformed into random boundaries. Thus, it is necessary to evaluate the thermal stability of the GBE-optimized GBCD of the materials. The GBE-treated alloy 800H samples were annealed at 500, 600, and 760 °C for 4 and 6 weeks. The as-received samples were annealed simultaneously along with the GBE samples as a reference. The GBCD of the annealed samples, which is plotted in Fig. 2(a), indicates that the GBCD was slightly changed by the anneal for both of the as-received and the

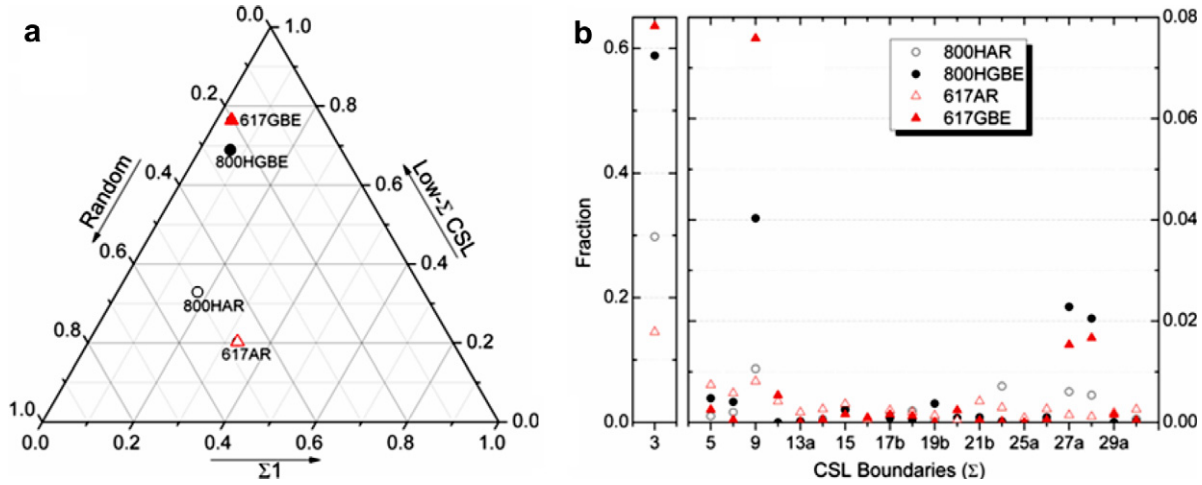

Fig. 1. (a) GBCD (fraction of Σ1, low-Σ CSL, and random boundaries) and (b) the fraction of low-Σ CSLBs ($3 \leqslant \Sigma \leqslant 29$) of alloy 800H and alloy 617 in the as-received (AR) and the GBE-treated conditions.

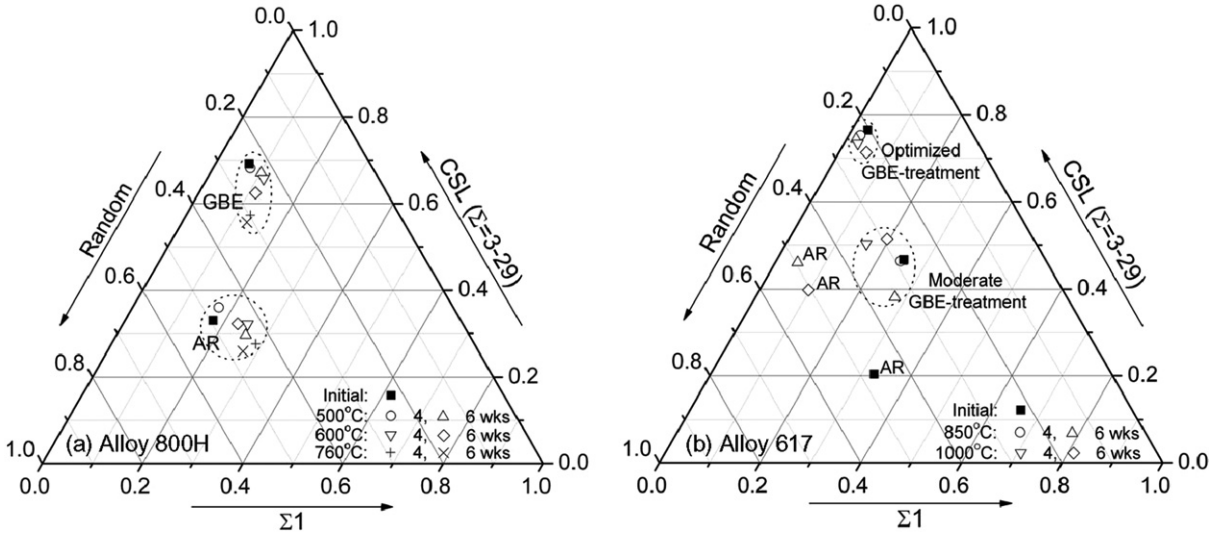

Fig. 2. Annealing effect on the GBCD (fraction of Σ1, low-Σ CSL, and random boundaries) of the as-received (AR) and the GBE-treated samples of (a) alloy 800H annealed at 500, 600, and 760 °C for 4 or 6 weeks and (b) alloy 617 annealed at 850 and 1000 °C for 4 or 6 weeks.

GBE-treated samples. The anneal at 760 °C (~58% melting temperature of alloy 800H) only slightly changed the GBCD of the GBE-treated samples.

Similar thermal stability testing was performed on the as-received and the GBE-treated alloy 617 samples by annealing at 850 and 1000 °C for 4 and 6 weeks. Samples with a moderate GBE-treatment were also tested at the same time. The GBCD of the annealed samples, which is plotted in Fig. 2(b), indicates that the GBCD of the as-received samples was changed significantly compared to the GBE-treated samples. This may result from the deformation-induced texture that contributed to the statistics of the Σ1 boundaries [8,14]. The GBCD of the samples with an optimized GBE-treatment was very stable at temperatures up to 1000 °C (~77% melting temperature of alloy 617) compared to that of the samples with a moderate GBE-treatment.

Therefore, the samples of alloys 800H and 617 with the optimized GBE-treatments are stable at their application temperatures up to 760 °C for alloy 800H and 1000 °C for alloy 617. Although the test time was limited to 6 weeks, the degradation rate of the GBCD of the optimally formed GBE-treated samples was very slow compared to the samples with moderate GBE-treatment.

3.2. Supercritical water (SCW) exposure tests

Both the as-received and the optimal GBE-treated alloy 800H and 617 samples were exposed to SCW to evaluate the GBE effect on the corrosion behavior.

3.2.1. Alloy 800H

After the SCW exposure at 500 and 600 °C for a variety of exposure times, the surface morphology of the samples was studied with optical microscope and SEM, the results of which are shown in Fig. 3. Extensive oxide exfoliation occurred on the as-received samples exposed to the SCW at 500 °C for 3 weeks (Fig. 3(a)) and 600 °C for 6 weeks (Fig. 3(c)). In contrast, the oxide scale is continuous and compact on the GBE-treated samples exposed to the SCW at 500 °C for 4 weeks (Fig. 3(b)) and 600 °C for 6 weeks (Fig. 3(d)).

To analyze the cause of the distinct difference, cross-section samples were prepared for microstructural analysis by means of EBSD. Fig. 4 shows the EBSD maps illustrating the distribution of phases and strain in the as-received and the GBE-treated samples exposed to the SCW at 500 °C for 3 weeks (Fig. 4(a) and (b)) and 4 weeks (Fig. 4(c) and (d)), respectively. Austenite (FCC structure), magnetite/spinel, and hematite were identified by the EBSD analysis as shown in Fig. 4(a). Magnetite and spinel are not differentiable by EBSD due to their identical crystal structure, but EDS analysis indicated that the inner layer is spinel and

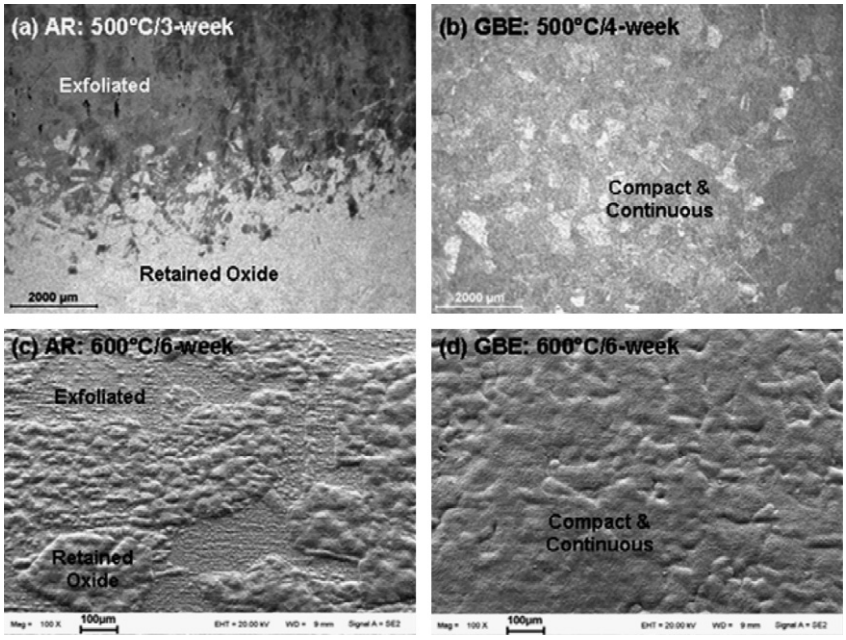

Fig. 3. Surface morphology of the as-received (AR) and the GBE-treated alloy 800H samples exposed to the SCW at 500 °C for 3 or 4 weeks (a, b: optical images) and 600 °C for 6 weeks (c, d: secondary electron images).

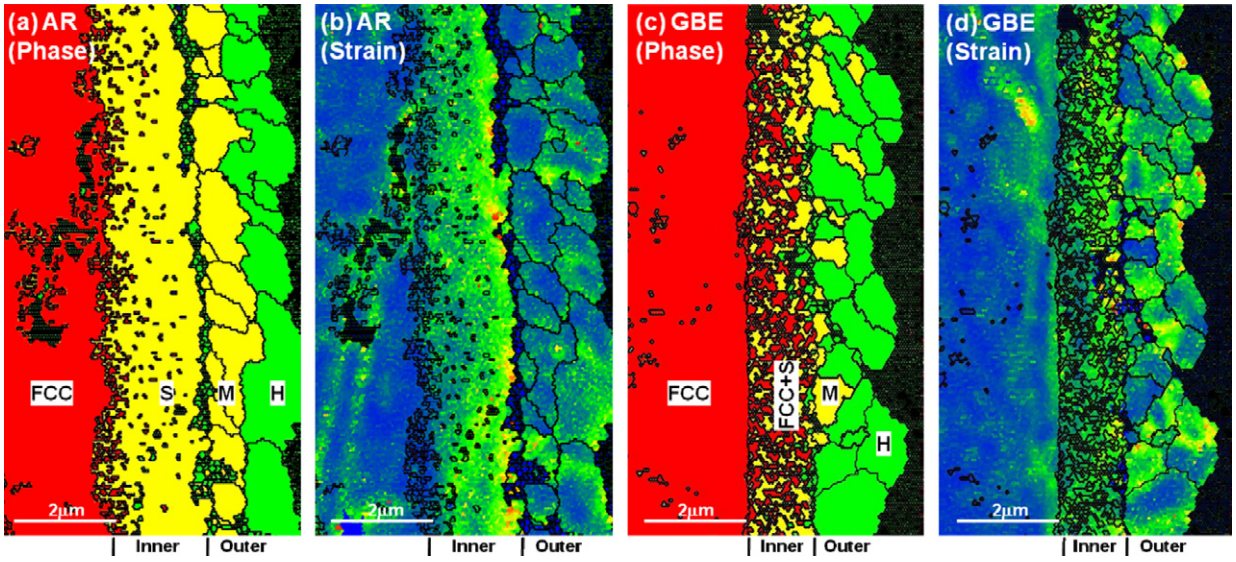

Fig. 4. EBSD maps of cross-section alloy 800H samples demonstrating the phase and strain (0–5° average misorientation) distribution: (a, b) the as-received (AR) samples exposed to the SCW at 500 °C for 3 weeks and (c, d) the GBE-treated samples exposed to the SCW at 500 °C for 4 weeks. The labels FCC, S, M, and H denote phases with face-centered cubic structure such as the substrate austenite, spinel [$(Fe,Cr)_3O_4$], magnetite [Fe_3O_4], and hematite [Fe_2O_3], respectively.

the outer layer is magnetite [12]. Compared to the as-received sample as shown in Fig. 4(a), the GBE-treated sample, as shown in Fig. 4(c), has an outer layer with a higher fraction of hematite mixed with a small amount of magnetite, and an inner layer with spinel mixed with phases identified as the austenite. The strain distribution as shown in Fig. 4(b) is presented by local average misorientation between each EBSD data point measurement and its neighbors excluding any higher angle boundaries (>5°). This figure indicates that there is a strain accumulation close to the spinel-magnetite interface (the interface between the inner and the outer layers). The strain distribution, as shown in Fig. 4(d), is relatively uniform in the oxide scale on the GBE-treated sample compared to that on the as-received sample. By integrating the strain intensity along the direction parallel to the spinel-magnetite interface, relative strain intensity as a function of the location across the oxide scale was obtained and is plotted in Fig. 5. It is clear that there is a sharper strain change at the spinel-magnetite interface in the as-received sample compared to that in the GBE-treated sample. The strain change at the spinel-magnetite interface on the GBE-treated sample is about 1/2 of that on the as-received sample. The sharper strain change in the oxide scale may have contributed to the extensive oxide exfoliation that occurred on the as-received sample.

As described in the Section 3.1, the only major microstructural change induced by the GBE treatments is the greatly increased fraction of low-Σ CSLBs and decreased fraction of random boundaries. Although there is also a decrease in the fraction of Σ1 boundaries, the effect of these boundaries on properties is smaller than the others [2]. Generally, grain boundaries are fast diffusion paths. The low energies associated with the high population of low-Σ CSLBs do not favor fast diffusion, and thus decrease the overall diffusivity along grain boundaries, shifting the grain boundary diffusivity much closer to the bulk diffusivity. The lower global diffusivity through the sample decreased the outward transport of Fe in the GBE-treated alloy 800H sample, resulting in less Fe supplied to the GBE-treated sample surface compared to that on the as-received sample. The reduced Fe resulted in a relatively higher oxygen activity promoting the formation of hematite instead of magnetite on the GBE-treated alloy 800H sample exposed to the SCW (Fig. 4(c)) [19]. Similarly, the inward diffusivity of O was also decreased in the GBE-treated sample, resulting in less oxidation in the inner layer of the oxide scale (Fig. 4(c)).

Fig. 6 shows the volume thermal expansion coefficient (α_v) of alloy 800H [11] and the specific oxides hematite, magnetite, and spinel [20]. The pressure effect on the thermal expansion coefficient is negligible due to the relatively low testing pressure (~25 MPa) and the similar bulk modulus of these oxides [21–23]. The α_v coefficients of hematite and spinel decrease with a similar trend in transitioning from the testing temperature to room temperature. However, the trend of the α_v of magnetite becomes significantly different from that of spinel and hematite for temperatures below ~400 °C. The significant difference in the α_V coefficients of magnetite and spinel may have led to the sharper strain change at the spinel-magnetite interface on the as-received sample (Figs. 4(b) and 5). While the smaller α_v difference between hematite and spinel as well as the decreased fraction of spinel may have alleviated the strain at the spinel-hematite interface on the GBE-treated sample (Figs. 4(d) and 5). Furthermore, hematite has a higher thermal conductivity (12.6 W/m-K) than magnetite (5.0 W/m-K) [24], which more rapidly dissipates heat and results in a higher strain intensity in the outer layer (hematite). This increased strain intensity in hematite further decreased the strain change at the inner–outer interface (the spinel-hematite

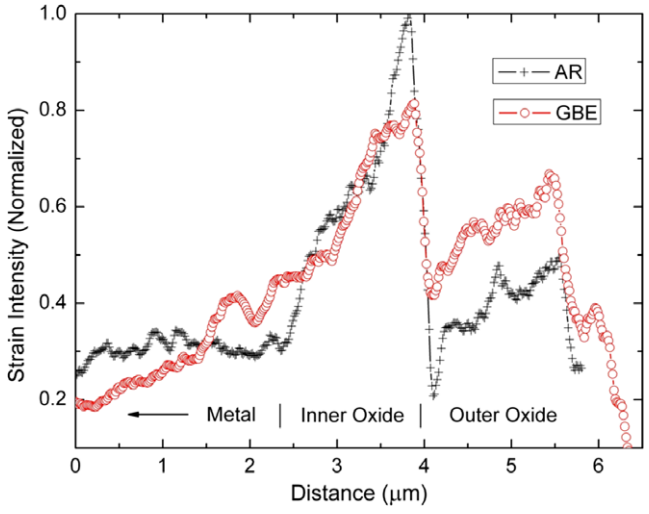

Fig. 5. Normalized strain intensity across the oxide scale on the as-received (AR) and the GBE-treated alloy 800H samples as shown in Fig. 4. The two lines are aligned at the inner–outer oxide interface.

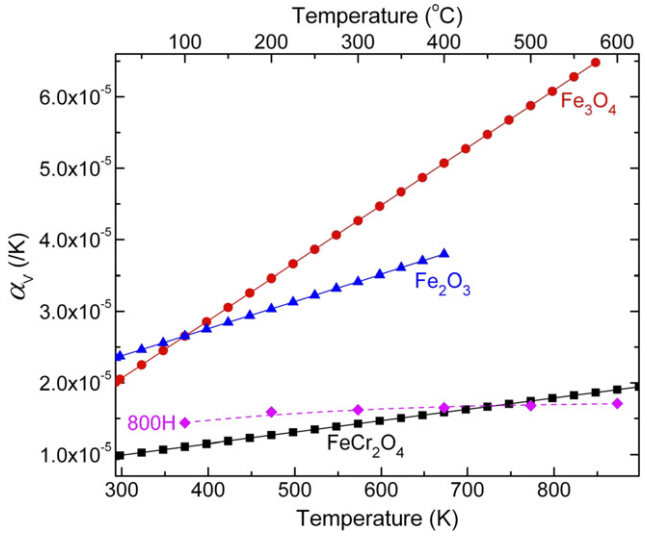

Fig. 6. Volume thermal expansion coefficient (α_v) of alloy 800H [11] and oxides such as Fe_2O_3 (hematite), Fe_3O_4 (magnetite), and $FeCr_2O_4$ (spinel) [20].

interface) on the GBE-treated sample (Fig. 5). The strain distribution (Fig. 5) and the α_v of the oxides (Fig. 6) support the experimental observations that the oxide exfoliation occurred mostly at the spinel-magnetite interface with a few at the magnetite–hematite interface in the as-received samples.

In addition to the sharper strain change, strong and anisotropic texture was observed in the oxide scale on the as-received sample [12]. In contrast, the texture in the oxide scale on the GBE-treated sample was isotropic and the texture intensity was ~18% of that on the as-received sample. The strong and anisotropic texture may have promoted the oxide exfoliation that occurred on the as-received sample due to the relationship among anisotropic texture, anisotropic grain boundary energy, and growth stress [12].

3.2.2. Alloy 617

The oxide scale formed on the SCW-exposed alloy 617 samples is less than ~100 nm. It is difficult to tell the thickness difference of the scales on the as-received and the GBE-treated samples from cross-section SEM analyses. Due to the thin oxide scale, grazing-incidence X-ray diffraction (GIXRD) was employed to identify the oxide phases. The GIXRD spectra of the as-received and the GBE-treated alloy 617 samples exposed to the SCW at 500 °C for 4 weeks are shown in Fig. 7, where 'A' denotes FCC phase from the substrate, 'C' denotes chromium oxide (Cr_2O_3, PDF# [38-1479]), and the unlabeled peaks denote spinel such as $(Ni,Co)Cr_2O_4$ (PDF# [23-1271] and [22-1084]). It is clear that oxide scales formed on both of the as-received and the GBE-treated samples are composed of chromium oxide and spinel. By comparing the relative peak intensity of the chromium oxide and the spinel, it is possible to deduce that the oxide scale on the GBE-treated sample has a higher fraction of chromium oxide than that on the as-received sample. Additionally, the GBE-treated sample shows a {111} texture in the substrate, which may have played a role on the oxide formation. The relationship between texture and grain boundary engineering has been briefly involved in Ref. [25].

Oxide surface chemistry of the SCW-exposed alloy 617 samples was analyzed by XPS instead of EDS due to the thin oxide scale. XPS surface survey profiles of the as-received and the GBE-treated samples are shown in Fig. 8. It is clear that Ni and Co are present on the as-received sample surface in addition to Cr and O on both the as-received and the GBE-treated sample surfaces. The other peaks correspond to Auger peaks and contaminants such as C and Ar. The presence of the Ni and Co on the as-received sample surface indicates that the oxide scale on the as-received sample is either composed of a discontinuous chromium oxide or complex oxides. In contrast, the GBE-treated sample surface is covered by a continuous chromium oxide. This observation is consistent with the GIXRD results as shown in Fig. 7 that the oxide scale on the GBE-treated sample has a higher fraction of chromium oxide than that on the as-received sample.

In Alloy 617, chromium was preferentially oxidized on the surface due to its higher concentration, higher diffusivity [26,27], and strong affinity for oxygen. As discussed in the previous section, the grain boundary diffusivity is expected to be much closer to the bulk diffusivity in the GBE-treated samples, which may have led to a relatively uniform diffusivity to the free surface. The uniform diffusion may have contributed to the formation of a continuous chromium oxide on the GBE-treated sample.

3.3. Cyclic oxidation tests

The weight changes of the as-received and the GBE-treated alloy 800H samples subjected to cyclic oxidation

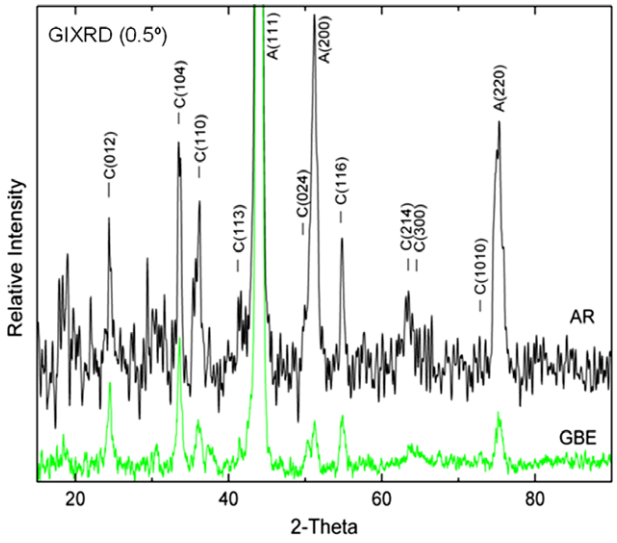

Fig. 7. Grazing incidence X-ray diffraction (GIXRD) patterns with an incident angle of 0.5° of the as-received (AR) and the GBE-treated alloy 617 samples exposed to the SCW at 500 °C for 4 weeks.

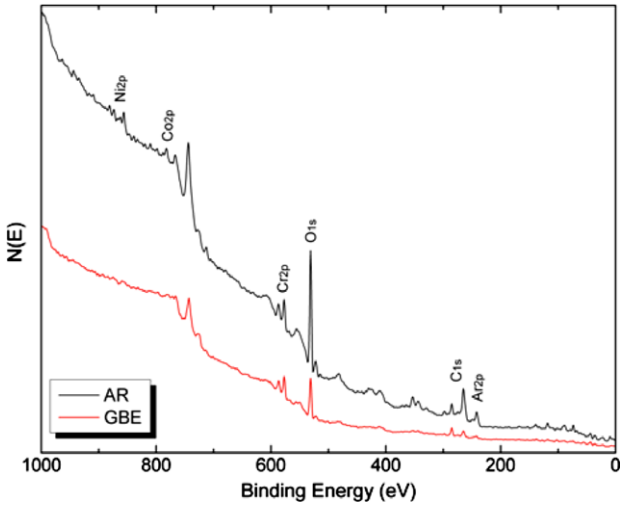

Fig. 8. X-ray photoelectron spectroscopy (XPS) surface survey spectra of the as-received (AR) and the GBE-treated alloy 617 samples exposed to the SCW at 500 °C for 4 weeks.

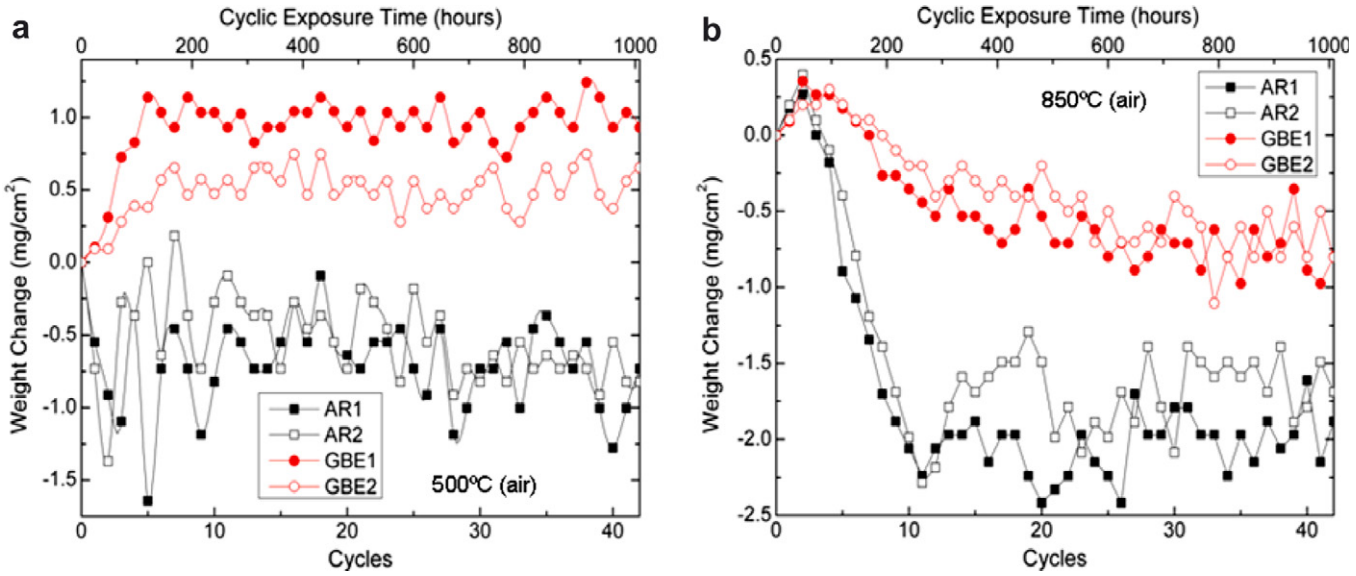

Fig. 9. Weight change of the as-received (AR) and the GBE-treated alloy 800H samples subjected to cyclic exposure in air at (a) 500 °C and (b) 850 °C.

tests in air at 500 and 850 °C for a total cyclic exposure time of 1008 h are shown in Fig. 9. The 500 °C test results as shown in Fig. 9(a) indicate that the GBE-treated samples had a weight gain, which was kept relatively constant with the cycles. In contrast, the as-received samples had a weight loss. The 850 °C test results as shown in Fig. 9(b) indicate that both the GBE-treated and the as-received samples had a short period of weight gain followed by a weight loss during the rest of the cyclic exposure testing. The weight loss of the GBE-treated samples was only ~40% of the as-received samples. More extensive exfoliation was observed on the as-received samples by SEM analyses. The cyclic oxidation test results indicate that the oxide exfoliation resistance of alloy 800H was greatly improved by the GBE-treatment.

Similarly, the weight changes of the as-received and the GBE-treated alloy 617 samples subjected to cyclic oxidation test in air at 850 and 1000 °C for a total cyclic exposure time of 1008 h are shown in Fig. 10. The 850 °C test results as shown in Fig. 10(a) indicate that the GBE-treated samples had a small weight gain and the weight gain was kept relatively constant with the cycles. In contrast, the as-received samples had a large weight gain, which is about 3 times of the GBE-treated samples, at the beginning part of the cyclic oxidation test, and the weight gain decreased with the cycles. The 1000 °C test results as shown in Fig. 10(b) indicate that both the GBE-treated and the as-received samples had a weight gain, but the weight gain of the GBE-treated samples was ~55% of the as-received samples. Exfolia-

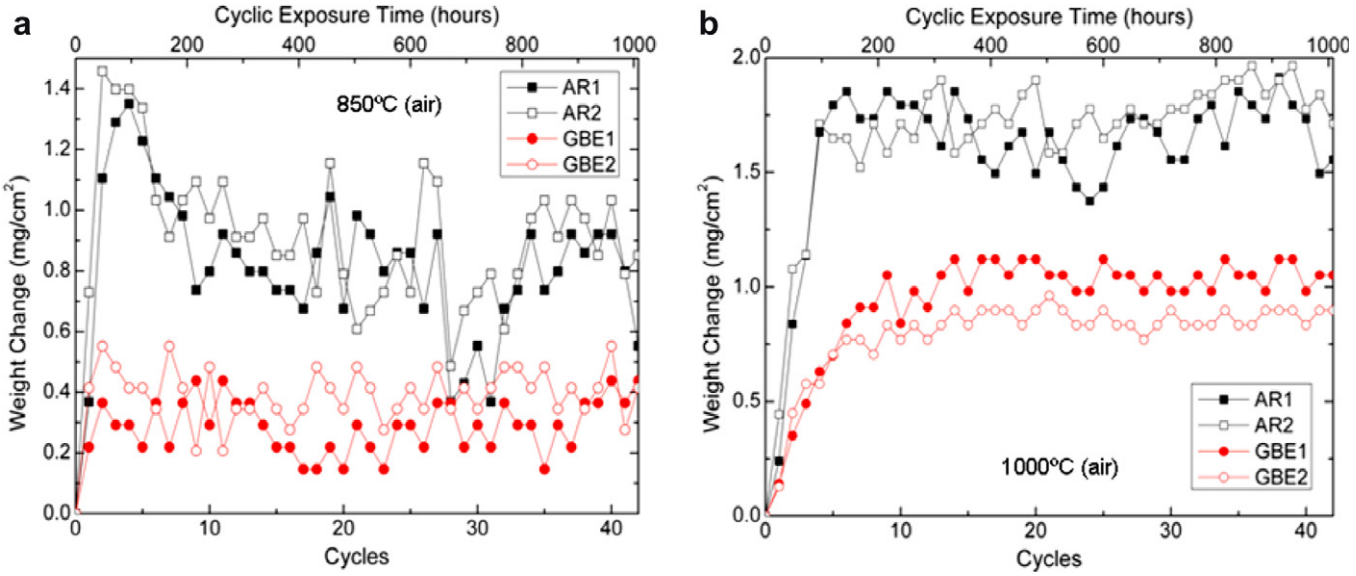

Fig. 10. Weight change of the as-received (AR) and the GBE-treated alloy 617 samples subjected to cyclic exposure in air at (a) 850 °C and (b) 1000 °C.

tion was only observed on the as-received alloy 617 samples cyclically exposed at 850 °C. The cyclic oxidation test results indicate that the oxide scale stability (relatively constant weight change) was greatly improved and the oxidation rate (weight gain) was greatly decreased by the GBE-treatment for alloy 617.

It is clear that the GBE-treatments played a significant effect on the cyclic oxidation performance of these two alloys. The microstructure of the cyclic oxidation-induced oxide scales on the as-received and the GBE-treated alloy 800H and alloy 617 samples are currently being studied and will be reported in future detailed work.

3.4. GBE effect on mechanical properties of alloy 800H

The effect of GBE on the strength and ductility of alloy 800H were evaluated utilizing impact and tensile testing.

3.4.1. Impact tests

The specimens subjected to the impact tests were not completely fractured into two pieces. The profiles of the impact test results of the as-received and the GBE-treated alloy 800H samples are shown in Fig. 11. The figure displays load versus test time and specimen deflection, which indicates that the GBE-treated samples experienced a higher load and a slightly shorter test time/smaller defection than the as-received samples. The analyzed data are summarized in Table 2. Impact strength was not calculated due to the unbroken specimens. The absorbed energy is about the same for the as-received and the GBE-treated samples, but the yield and the ultimate load of the GBE-treated samples were increased more than 10% compared to those of the as-received samples. Since the major change induced by the GBE-treatment on the alloy 800H was GBCD, the increased yield and ultimate loads of the GBE-treated samples were believed to be attributable to the greatly increased fraction of low-energy low-Σ CSLBs.

Table 2
Impact test results of alloy 800H samples in the as-received (AR) and the GBE-treated conditions

Sample	Load (N)		Total time (ms)	Absorbed energy (J)
	Yield	Ultimate		
AR	805 (33)	1234 (25)	17.5 (0.2)	24.9 (0.3)
GBE	921 (33)	1400 (41)	16.7 (0.4)	24.2 (0.5)
Changes	14.4%	13.5%	−4.6%	−2.8%

The numbers in parentheses are standard deviations.

3.4.2. Tensile tests

The tensile test profiles are plotted in Fig. 12. The results for the specimens irradiated at 660 °C show only a slight increase in yield strength (YS) and ultimate tensile strength (UTS) and a slight decrease in uniform and total elongations for the GBE-treated specimen compared to the values for the specimen in the as-received condition. The GBE-treated specimen irradiated at 580 °C demonstrated a significant increase in both YS and UTS with only slight decreases in uniform and total elongation compared to the results for the as-received specimen irradiated at 580 °C. The analyzed tensile data are summarized in Table 3.

Since all other experimental parameters (dose, irradiation temperature, test temperature, etc.) between the GBE-treated and the as-received specimens remain unchanged, the enhanced strength observed in the GBE-treated specimen irradiated at 580 °C is attributed to the GBE-treatment. The GBE-treated specimen irradiated at 660 °C did exhibit some increase in YS (14%) compared to the as-received specimen irradiated at 660 °C. However, the magnitude of the change in YS observed between the GBE-treated and the

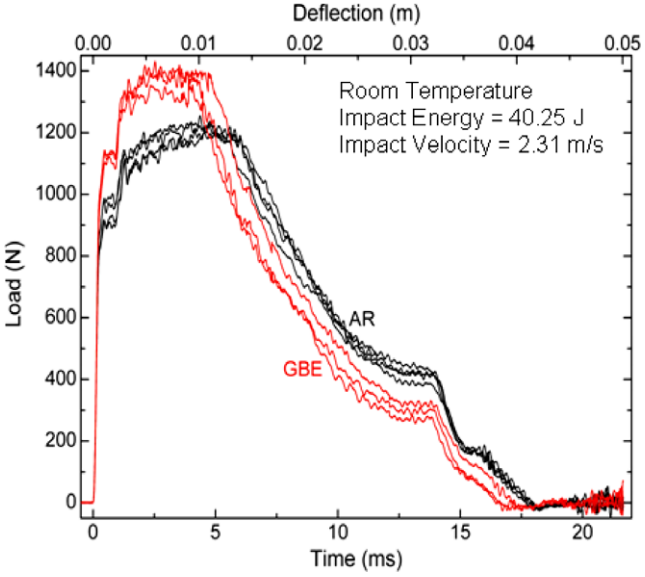

Fig. 11. Room temperature impact test results of the as-received (AR) and the GBE-treated alloy 800H samples.

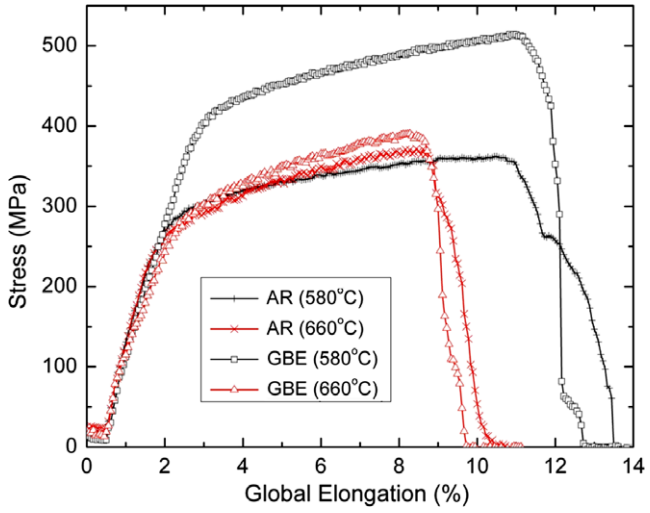

Fig. 12. Tensile test profiles of the as-received (AR) and the GBE-treated alloy 800H specimens tested at 580 and 660 °C, which were subjected to neutron irradiation at the same temperatures.

Table 3
Tensile test results of the as-received (AR) and the GBE-treated alloy 800H specimens tested at 580 and 660 °C, which were subjected to neutron irradiation at the same temperatures

Irradiation/test temperature (°C)	Specimen	Yield stress (MPa)	Ultimate stress (MPa)	Failure stress (MPa)	Total elongation (%)	Uniform elongation (%)
580	AR	272.0	362.4	60.9	12.9	8.05
	GBE	503.7	514.4	52.9	11.8	7.34
	Changes	48.5%	42.0%	−13.2%	−8.5%	−8.8%
660	AR	249.4	371.9	38.7	9.55	6.11
	GBE	283.8	390.3	48.3	9.19	5.04
	Changes	13.8%	4.9%	24.8%	−3.8%	−17.5%

as-received specimens irradiated at 580 °C (49%) was more than three times the increase in YS of the specimens irradiated at 660 °C (14%). The difference in the magnitude of increase in UTS values between the GBE-treated and the as-received specimens irradiated at 580 °C and those irradiated at 660 °C was found to be greater than the YS difference; with the specimens irradiated at 580 °C exhibiting an increase in UTS (42%) of more than eight times the increase in UTS (5%) for those specimens irradiated at 660 °C. While a reduction in ductility of all irradiated specimens examined was attributed to microstructural changes imposed by neutron irradiation [28], the slight reduction in ductility between the GBE-treated and the as-received specimens is attributed to the GBE-treatment. The difference in radiation hardening and reduction-in-ductility behavior between the two irradiation temperatures indicates that the effect of the GBE-treatment appears to be dependent on material temperature during irradiation. Detailed microstructural evolution induced by neutron irradiation and thermal annealing on the as-received and the GBE-treated specimens will be explored in future studies to better understand the effect of radiation and temperature on GBE strengthening effectiveness during exposure to radiation.

4. Conclusions

Grain boundary engineering (GBE) was performed on Incoloy 800H and Inconel 617 samples by means of thermomechanical processing. The GBE-improved grain boundary character distribution (significantly increased fraction of low-Σ CSLBs and decreased random boundaries) in the alloys 800H and 617 are thermally stable at temperatures up to 760 °C for the alloy 800H and 1000 °C for the alloy 617 for times on the order of 1000 h. The effect of the GBE treatments on the properties of materials such as corrosion resistance and strength was evaluated using supercritical water (SCW) exposure tests, cyclic oxidation tests, impact tests, and tensile tests after neutron irradiation. The GBE treatment significantly mitigated the oxide exfoliation of alloy 800H. The microstructural analysis of the SCW-exposed alloy 800H samples indicates that the oxide scale on the as-received sample has a sharper strain change and anisotropic strong texture compared to that on the GBE-treated samples, which led to the oxide exfoliation that occurred on the as-received samples. The GBE treatment reduced the oxidation rate (weight gain) to ~1/2 of the as-received alloy 617 as evaluated by the cyclic oxidation tests in air at 1000 °C. The SCW exposure results indicate that the GBE-treatment resulted in a more compact oxide scale with a continuous chromium oxide surface layer compared to the as-received alloy 617 samples. In addition to the improved corrosion resistance, the impact testing indicated that the GBE treatment enhanced by more than 10% the strength of alloy 800H at room temperature. The GBE-treatment appears to have enhanced high-temperature yield and ultimate strengths following exposure to radiation compared to the as-received condition, while not significantly reducing the material's ductility. About a 49% at 580 °C and ~14% at 660 °C enhancement in yield strength and ~9% at 580 °C and ~4% at 660 °C loss in total elongation were observed in the GBE-treated alloy 800H samples compared to the as-received samples. However, the material temperature during irradiation appears to have a strong influence on the effectiveness of GBE-treatment with respect to strengthening and will require further investigation to fully understand.

Acknowledgements

This work is supported by the DOE Generation IV initiative program, NACE, and the Office of Naval Research (ONR). Thanks also give to Special Metals Inc. for supplying the Inconel alloy 617 for this study.

References

[1] P.E.J. Flewitt, R.K. Wild, Grain Boundaries – Their Microstructure and Chemistry, John Wiley & Sons Ltd., England, 2001.
[2] V. Randle, The Role of the Coincidence Site Lattice in Grain Boundary Engineering, The Institute of Materials, London, 1996.
[3] U. Erb, P. Lin, S. Kim, K.T. Aust, F. Gonzalez, G. Palumbo, in: T.S. Srivatsan, R.A. Varin (Eds.), Proceedings of the 10th International Symposium on Processing and Fabrication of Advanced Materials, Indianapolis, IN, USA, 5–8 November, 2001, p. 3.
[4] D.S. Lee, H.S. Ryoo, S.K. Hwang, Mater. Sci. Eng. A 354 (2003) 106.
[5] E.M. Lehockey, G. Palumbo, P. Lin, Metall. Mater. Trans. A 29 (1998) 3069.
[6] M. Shimada, H. Kokawa, Z.J. Wang, Y.S. Sato, I. Karibe, Acta Mater. 50 (2002) 2331.

[7] Y. Pan, B.L. Adams, T. Olson, N. Panayotou, Acta Mater. 44 (1996) 4685.
[8] V.Y. Gertsman, S.M. Bruemmer, Acta Mater. 49 (2001) 1589.
[9] V. Randle, Acta Mater. 47 (1999) 4187.
[10] A Technology Roadmap for Generation IV Nuclear Energy Systems, US DOE Nuclear Energy Research Advisory Committee and the Generation IV International Forum, December 2002 (<http://gif.inel.gov/roadmap/>).
[11] Special Metals Publication: SMC-047, 2004 (alloy 800H) and SMC-029, 2005 (alloy 617) (<http://www.specialmetals.com>).
[12] L. Tan, K. Sridharan, T.R. Allen, J. Nucl. Mater. 348 (2006) 263.
[13] P. Billot, D. Barbier, in: 2nd International Topical Meeting on High Temperature Reactor Technology, Beijing, China, September 22–24, 2004, paper #A01.
[14] L. Tan, T.R. Allen, Metall. Mater. Trans. A 36 (2005) 1921.
[15] L. Tan, K. Sridharan, T.R. Allen, J. Nucl. Mater. 371 (2007) 171.
[16] ASTM E 23 – 06: Standard test methods for notched bar impact testing of metallic materials, ASTM International, West Conshohocken, PA, USA.
[17] L.L. Snead, A.M. Williams, A.L. Qualls, in: M.L. Grossbeck (Ed.), Effects of Radiation on Materials: 21st International Symposium, ASTM Special Technical Publication STP1447, January 2004, paper # STP11262S.
[18] G. Palumbo, K.T. Aust, U. Erb, P.J. King, A.M. Brennenstuhl, P.C. Lichtenberger, Phys. Status Solidi A 131 (1992) 425.
[19] R.M. Cornell, U. Schwertmann, The Iron Oxides – Structure, Properties, Reactions, Occurrences and Uses, 2nd Ed., Wiley-VCH Verlag GmbH & Co. KGaA, Germany, 2003.
[20] B.J. Skinner, in: S.P. Clark, Jr. (Ed.), Handbook of Physical Constants, Geol. Soc. Am. Mem., 1966, p. 75.
[21] Y. Fei, in: Mineral Physics and Crystallography – A Handbook of Physical Constants, the American Geophysical Union Reference Shelf 2, 1995.
[22] C. Haavik, S. Stølen, H. Fjellvåg, M. Hanfland, D. Häusermann, Am. Mineral. 85 (2000) 514.
[23] H.J. Reichmann, S.D. Jacobsen, Am. Mineral. 91 (2006) 1049.
[24] A.L. Edwards, For Computer Heat-Conduction Calculations A Compilation of Thermal Properties Data, UCRL-50589, February 24, 1969.
[25] T. Watanabe, S. Tsurekawa, Acta Mater. 47 (1999) 4171.
[26] C.E. Campbell, W.J. Boettinger, U.R. Kattner, Acta Mater. 50 (2002) 775.
[27] S.J. Rothman, L.J. Nowicki, G.E. Murch, J. Phys. F: Metal Phys. 10 (1980) 383.
[28] J.R. Lindgren, Nucl. Technol. 66 (1984) 607.